Improving AR-SSVEP Recognition Accuracy Under High Ambient Brightness Through Iterative Learning

Rui Zhang, Lijun Cao, Zongxin Xu, Yangsong Zhang, Lipeng Zhang, Yuxia Hu, Mingming Chen, and Dezhong Yao

***Abstract*— Augmented reality-based brain-computer interface (AR-BCI) system is one of the important ways to promote BCI technology outside of the laboratory due to its portability and mobility, but its performance in real-world scenarios has not been fully studied. In the current study, we first investigated the effect of ambient brightness on AR-BCI performance. 5 different light intensities were set as experimental conditions to simulate typical brightness in real scenes, while the same steady-state visual evoked potentials (SSVEP) stimulus was displayed in the AR glass. The data analysis results showed that SSVEP can be evoked under all 5 light intensities, but the response intensity became weaker when the brightness increased. The recognition accuracies of AR-SSVEP were negatively correlated to light intensity, the highest accuracies were 89.35% with FBCCA and 83.33% with CCA under 0 lux light intensity, while they decreased to 62.53% and 49.24% under 1200 lux. To solve the accuracy loss problem in high ambient brightness, we further designed a SSVEP recognition algorithm with iterative learning capability, named ensemble online adaptive CCA (eOACCA). The main strategy is to provide initial filters for high-intensity data by iteratively learning low-light-intensity AR-SSVEP data. The experimental results showed that the eOACCA algorithm had significant advantages under higher light intensities (>600 lux). Compared with FBCCA, the accuracy of eOACCA under 1200 lux was increased by 13.91%. In conclusion, the current study contributed to the in-depth understanding of the performance variations of AR-BCI under different lighting conditions, and was helpful in promoting the AR-BCI application in complex lighting environments.**

***Index Terms*— Brain–computer interface (BCI), steady-state visual evoked potentials (SSVEP), light intensity, augmented reality (AR), iterative learning.**

Manuscript received 28 November 2022; revised 2 March 2023; accepted 13 March 2023. Date of publication 23 March 2023; date of current version 28 March 2023. This work was supported in part by the STI 2030-Major Project under Grant 2022ZD0208500, in part by the Technology Project of Henan Province under Grant 222102310031, and in part by the National Natural Science Foundation of China under Grant 62173310. *(Corresponding authors: Dezhong Yao; Mingming Chen.)*

This work involved human subjects or animals in its research. Approval of all ethical and experimental procedures and protocols was granted by the Life Science Ethics Review Committee of Zhengzhou University under Approval No. ZZUIRB2021-92, and performed in line with the Declaration of Helsinki.

Rui Zhang, Lijun Cao, Zongxin Xu, Lipeng Zhang, Yuxia Hu, and Mingming Chen are with the Henan Key Laboratory of Brain Science and Brain–Computer Interface Technology, School of Electrical and Information Engineering, Zhengzhou University, Zhengzhou 450001, China (e-mail: mmchen@zzu.edu.cn).

Yangsong Zhang is with the School of Computer Science and Technology, Southwest University of Science and Technology, Mianyang 621010, China.

Dezhong Yao is with the Henan Key Laboratory of Brain Science and Brain–Computer Interface Technology, School of Electrical and Information Engineering, Zhengzhou University, Zhengzhou 450001, China, and also with the Clinical Hospital of Chengdu Brain Science Institute, MOE Key Laboratory for Neuroinformation, University of Electronic Science and Technology of China, Chengdu 611731, China (e-mail: dyao@uestc.edu.cn).

Digital Object Identifier 10.1109/TNSRE.2023.3260842

I. Introduction

BRAIN-COMPUTER Interface (BCI) is a new type of technology that enables humans or other animals to directly connect the brain with the external environment without the aid of peripheral nerves and muscles, enabling the brain to directly control external equipment [1]. It builds a new way of communication between the brain and external devices [2]. The human cerebral cortex is widely distributed with multiple networks with different resonant frequencies. When subjected to a repeated stimulus with a constant external frequency, the network corresponding to the stimulus frequency or harmonic will be synchronized, so that steady-state visual evoked potentials (SSVEP) are generated in the brain scalp [3], [4]. The SSVEP of different frequencies can be evoked by stimuli of different frequencies, and BCI can directly output brain intent by decoding SSVEP. Compared with other types of BCI, SSVEP-BCI has the advantages of high accuracy, high signal-to-noise ratio (SNR), high information transfer rate (ITR), and less subject training, which makes it one of the most commonly used BCI control systems [5], [6].

In the traditional SSVEP-BCI system, most of the flicker stimuli of SSVEP are presented on the computer screen (CS) [7]. Due to the relatively fixed position and large size of the device, users can only sit or stand in a specific room to complete interactive tasks, and it greatly limits the scope of application of the system. During the experiment, the subjects need to shift their attention back and forth between the stimulus screen and the normal visual field, which increases the experimental burden of the subjects [8].

In recent years, with the continuous development of augmented reality (AR) technology, AR glass has gradually entered our lives. It integrates the key components of AR technology on glasses, and this greatly improves portability and practicability. AR glass uses projection technology to superimpose virtual things in people's real vision field, thus virtual things and the real external environment can be observed simultaneously [9]. According to the way that AR superimposes virtual images on the real environment, it can be divided into video see-through AR (VST-AR), optical see-through AR (OST-AR), and projection AR [10]. Compared with the two other types, OST-AR utilizes the principle of reflection of light to directly fuse virtual information into the real environment through optical elements fixed in front of the user's eyes, thereby providing a more realistic AR experience. As early as the 1990s, Caudell et al. realized the first OST-AR glass device [11]. Due to the manufacturing cost at that time, it has not been widely studied. In 2015, Microsoft released an OST-AR glass, Hololens, which brought AR glass back into the public's attention.

At present, BCI technology faces two important challenges in practical application: the non-portable EEG acquisition and stimulus presentation equipment, and the unnatural BC interaction mode [12]. Coupled with the development of wireless EEG signals acquisition equipment, AR may become the best way to bring the BCI system out of the laboratory into the real environment. In the SSVEP-BCI system based on AR technology, the stimulus interface of SSVEP can be projected in the real environment by AR glass, getting rid of various limitations of CS display. It achieves the purpose of being portable and wearable [13], making users more natural and comfortable interacting with the outside world. The application of AR technology could greatly expand the research field of the SSVEP-BCI system and broaden its application scenarios.

However, many studies have confirmed that the performance of AR-SSVEP system was significantly different from that of traditional CS-SSVEP system. Ke et al. designed an 8-target SSVEP-BCI system with AR glass, and compared the performance differences between AR-BCI and CS-BCI. The results showed that the accuracy of AR-BCI was lower than that of CS-BCI [14]. Zhao et al. designed visual stimulus paradigms with different layouts, compared the signals characteristics of AR-SSVEP and CS-SSVEP in a shielded room in the laboratory, and found that the performance of AR-SSVEP can be affected by the stimulus layouts, while CS-SSVEP not [15]. Our previous study tested the performance of AR-SSVEP and CS-SSVEP under different numbers of stimuli. The results indicated a significant difference in recognition performance between the two stimulus presentation methods, and the increase in stimulus number will cause a decrease in the recognition accuracy of AR-SSVEP [16]. Besides, Ravi et al. also confirmed that dynamic background would reduce the performance of AR-SSVEP under laboratory conditions [17]. Zhang et al. completed a robotic control system based on dynamic stimulus and also found that the classification accuracy was negatively correlated to the moving speed of the target [18]. These studies indicated that the robustness of AR-SSVEP is not as strong as that of traditional CS-SSVEP, and it is easily affected by various factors.

Currently, the algorithms used to recognize AR-SSVEP is mainly derived from the commonly used algorithms in CS-SSVEP. Canonical correlation analysis (CCA) algorithm calculates the correlation between the experimental EEG and the template signals, and then output the identified target according to the correlation coefficients [19]. Filter bank based CCA (FBCCA) further divides EEG signals into multiple subbands, so that the information at the harmonics of the EEG signals can be effectively used to improve the recognition accuracy [20]. Task related component analysis (TRCA) finds an optimal weight coefficients to maximize the reproducibility of SSVEPs across multiple trials, leading to significantly enhanced SNR of SSVEPs [21]. The EEG data processed by these algorithms are often collected under fixed conditions, and they do not need to consider the impact of environmental factors for CS-SSVEP. However, when using AR devices as SSVEP stimulus presentation devices, especially outside the laboratory, the collected EEG data is faced with the interference of various environmental factors, which requires the algorithms for processing AR-SSVEP data to be adaptable to the environment. Several online adaptation schemes have been proposed to adjust the spatial filter [22], data length [23], stimulus size [24], or SSVEP template [25] for improving the CS-SSVEP recognition performance. So far, such online adaptation schemes have not been tested in AR-SSVEP experiment, and there is also a lack of online learning strategies for SSVEP characteristic changes caused by environmental factors.

With the extensive study of AR-BCI technology, researchers are eager to apply it in non-laboratory conditions and provide a better user experience. However, one of the key factors in non-laboratory conditions is the ambient brightness variations, and it is mostly set to be dark to avoid the influence on the AR-BCI experiment. Furthermore, besides the display system of the AR glass [26], the ambient brightness also affects human vision [27]. To the best of our knowledge, the effect of ambient brightness on AR-BCI and its influencing mechanism have not been studied, and there is also a lack of effective solutions to improve the performance robustness of AR-BCI under different light intensities, which greatly limits the application and development of AR-BCI.

In the current work, the ambient brightness was considered as the main factor, and five light intensities were set according to the typical application scenarios of AR-BCI. We investigated how ambient brightness affects AR-BCI performance at first. Then, inspired by online adaptive CCA (OACCA) [22], this paper further proposed a new algorithm framework which named ensemble OACCA (eOACCA) to adapt to the influence of environmental factors on the signal characteristics of AR-SSVEP. eOACCA not only learns the information of different targets under the same light intensity, but also learns the information of data under other light intensities, so that the spatial filters obtained at low light intensities can be used to enhance the spatial filters at high light intensities.

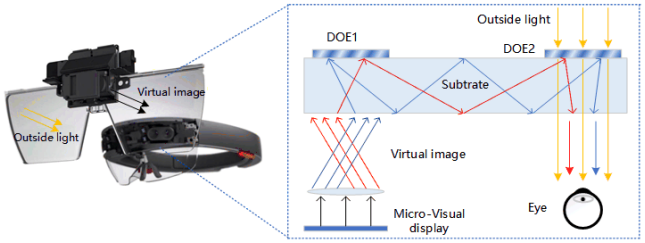

Fig. 1. Schematic diagram of optical waveguide principle. DOEs are diffractive optical elements. The virtual image passes through the convex lens into the glass substrate, the image is transmitted in the glass substrate by total reflection, and finally enters the human eyes. Note that external light can also enter the human eyes through the glasses.

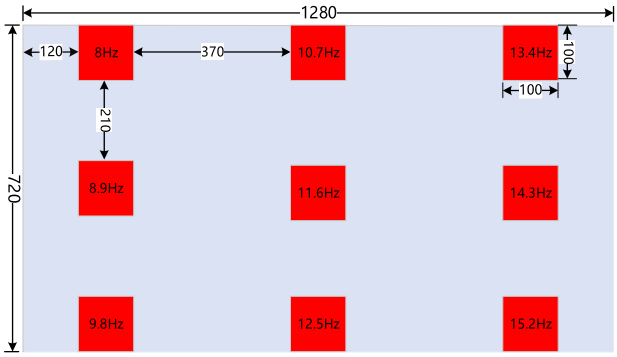

Fig. 2. Spatial and frequency layout of SSVEP stimulus. The lengths unit is pixels. There are no numbers on the stimulus during the experiment.

II. Materials and Methods

A. Experimental Paradigm and Data Acquisition

1) Stimulus Presentation and EEG Acquisition Equipment: The Hololens1 developed by Microsoft Corporation of the United States was used as the stimulus presentation device. The Hololens1 was an OST AR glass, which used digital light processing (DLP) projection technology to display virtual things. The key technology of Hololens 1 was the optical waveguide, as shown in Figure 1.

HoloLens1 provides users with a larger field of view through a 3-layer waveguide [28]. The total reflection of the optical waveguide ensured high definition and high contrast of image. This characteristic of the optical waveguide had a great advantage in optimizing the layout and beautifying the appearance of the headset. With the transmission channel of the waveguide, the display screen and imaging system could be moved away from the glasses to the top or side of the forehead. It greatly reduced the obstruction of the optical system to the outside world, and it also made the weight distribution of AR glass more ergonomic, improving the wearing experience of users.

The SynAmps2 amplifier produced by NeuroScan of the United States was used as EEG signals acquisition equipment. A total of 64 electrodes were selected to record.

EEG signals and placed according to the international standard 10-20 system. All electrodes were referenced to the Cz electrode, and the impedance was kept below 10 kΩ during recording. The sampling frequency of EEG signals was 1000 Hz.

2) Stimulus Paradigm and Lighting Environment Design: The visual flickering stimuli were presented to subjects by HoloLens 1 AR glass. The screen resolution of AR glass was 1280*720 pixels, and the refresh rate was 60 Hz. The visual stimuli were constructed using sampled sinusoidal coding [29], [30], and the stimulus layout and stimulus frequency were shown in Figure 2.

In this experiment, according to the brightness in several typical scenarios, experimental environments with different light intensities were set. Generally, the light intensities requirement of common learning places is 300 lux, and the brightness of international sports venues is about 1000 lux-1400 lux, the light requirement for the examination rooms in hospitals is generally 300-500 lux [31], the light of room in the sunny day is about 100-1000 lux, and at night is about 0.2 lux. According to the range of light intensity

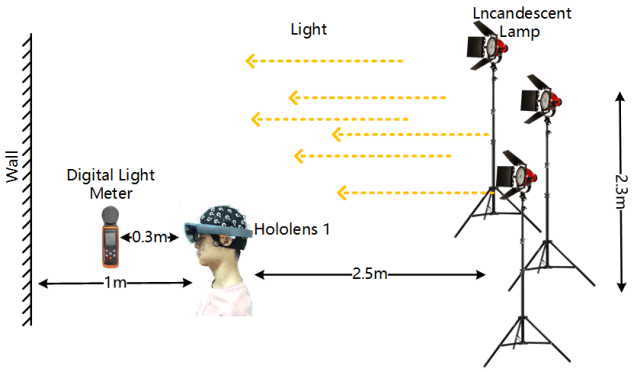

Fig. 3. Schematic diagram of the experimental environment with different light intensities.

variation in these scenes, we set the light intensity to 0 lux, 300 lux, 600 lux, 900 lux and 1200 lux in the experimental design. And three 800 W incandescent lamps were used as the light source, and a small shielded room was chosen for the experiment. The experimental environment was shown in Figure 3.

In order to ensure the uniformity of illumination in the experimental environment, three incandescent lamps were placed in the shielded room with an interval of about 1.2 m. We adopted the method of filling the light behind the experimenter's back to ensure that the subjects could carry out the experiment safely and normally, and the light source was set at about 2.5 m from the subjects' back. When the subject performed AR-SSVEP experiments using the AR glass, the light intensity was measured at about 30 cm in front of the subjects' eyes, which was the direction of light entered the human eyes. The light intensity measurement equipment was Victor VC1010C digital illuminometer, its measurement range was 0-20000 lux and the resolution was 0.1 lux. To ensure the measurement accuracy, the allowable error of light intensity was ±10 lux during the experiment.

3) Experiment and Data Collection: Twenty subjects with normal or corrected-to-normal vision (8 females and 12 males, aged 21-25 years) were recruited for this experiment, and all signed an informed consent form before the experiment. Two male subjects were excluded because the impedance could not be reduced below 10 kΩ. To avoid the adaptation factor,

we divided the subjects equally into two groups, one group used an increasing sequence of light intensities during the experiment, starting from 0 lux and ending with 1200 lux. The other group used a decreasing sequence of light intensities, starting from 1200 lux and ending with 0 lux. For each light intensity, subjects were asked to perform 8 trials, and each trial contained the 9 stimulus which described in Figure 2. At the beginning of each stimulus, the AR glass would give a target cue of 0.5 s, and then all the stimulus targets would start to flicker for 3 s, followed by a 2-s rest time. The subjects were required to move their gaze to the designated target stimulus during the cue time, and try not to blink during the flickering period. In each trial, subjects were required to gaze at the 9 targets in sequence according to the cue. We extracted EEG data during target flickering for the following analysis.

B. Data Processing and Analysis

The EEG data on the Oz channel of the occipital region was used for frequency domain analysis. First, the 3 s EEG data during the flickering time were segmented, then they were transferred from the time domain to the frequency domain by fast Fourier transform (FFT) to obtain the spectrogram. The SNR was calculated using the spectral value of the target frequency and the average spectral value of the left and right 2 Hz [16].

Two typical algorithms, canonical correlation analysis (CCA) [19] and filter bank based CCA (FBCCA) [20], were selected to recognize SSVEP. The ITR was used to evaluate the communication rate of the BCI system [32].

C. Design of the eOACCA Algorithm

In order to make the recognition algorithm of SSVEP adapt to the change of light intensity, we proposed a new optimization algorithm, ensemble online adaptive CCA (eOACCA). The algorithm was based on OACCA [22], but provided an initial parameter for the iterative learning of prototype spatial filters (PSF) and online multi-stimulus CCA(OMSCCA) with the help of data under other light conditions. Thus, it could learn not only the features of different target data, but also the features of data under different light conditions to further optimize and correct the filters. In addition, we also used the first-target optimization strategy for the target data to obtain a relatively accurate filter model at the beginning of filter learning. During the data processing, the idea of sub-band filtering was used to improve its accuracy.

1) Prototype Spatial Filters: Lao et al. [33] found a task-relevant common filter from different target data, which can effectively improve the recognition accuracy of SSVEP. After CCA calculation, each target would generate a recognition result $\hat{k}^{[t]}$ and corresponding filter $u_{\hat{k}^{[t]}}^{[t]}$, where $\hat{k}^{[t]}$ is the label classified by CCA algorithm, t represents the t-th target. For convenience, let $\tilde{u}^{[t]} = u_{\hat{k}^{[t]}}^{[t]} / ||u_{\hat{k}^{[t]}}^{[t]}||$, then a common filter u_0 was obtained from them. In [22], Wong et al. improved PSF into online learning mode, and they found a filter $u_0^{[t+1]}$ from $\tilde{u}^{[t]}$ of the previous target such that $u_0^{[t+1]}$ had the maximum similarity to $\tilde{u}^{[t]}$. As shown in equation (1)

$$\begin{aligned} \mathrm{u}_0^{[t+1]} &= \mathrm{argmax}_u \frac{\mathrm{u}^{\mathrm{T}} \sum_{m=1}^{t} \tilde{u}^{[\mathrm{m}]} \left(\tilde{u}^{[\mathrm{m}]}\right)^{\mathrm{T}} \mathrm{u}}{\mathrm{u}^{\mathrm{T}} \cdot \mathrm{u}} \\ &= \mathrm{argmax}_u \frac{\mathrm{u}^{\mathrm{T}} \mathrm{S}^{[\mathrm{t}]} \mathrm{u}}{\mathrm{u}^{\mathrm{T}} \cdot \mathrm{u}} \end{aligned} \tag{1}$$

As $S^{[t]} = \sum_{m=1}^{t} \tilde{u}^{[m]} (\tilde{u}^{[m]})^T$, each target recognition would adjust the next one $u_0^{[t+1]}$ to achieve the goal of continuous optimization and learning.

The eOACCA algorithm we proposed not only used $S^{[t]}$ to calculate the filter $u_0^{[t+1]}$, but also used the parameter S generated by data under other lighting conditions. Thus formula (1) can be rewritten as formula (2):

$$\mathrm{u}_0^{[t+1]} = \mathrm{argmax}_{\mathrm{u}} \frac{\mathrm{u}^{\mathrm{T}} (\mathrm{S} + \mathrm{S}^{[\mathrm{t}]}) \mathrm{u}}{\mathrm{u}^{\mathrm{T}} \mathrm{u}} \tag{2}$$

where $S + S^{[t]} = \sum_{i=1}^{n-1} \sum_{m=1}^{t} u_{0i}^m + \sum_{m=1}^{t} \tilde{u}_n^m (\tilde{u}_n^m)^T$, n was the index of different lighting conditions, and m was the index of the target.

2) Multi-Stimulus CCA: Wong et al. proposed an MSCCA algorithm [34], which aimed to learn a common spatial filter (w_x or w_y) from the subject's multi-stimulus SSVEP template. Then they changed the original batch learning mode to an online learning mode, forming an online MSCCA(OMSCCA) in the OACCA algorithm. Therefore, for the t-th test, the filter can be calculated by formula (3)

$$\begin{aligned} \left\{w_x^{[t+1]}, w_y^{[t+1]}\right\} &= \max_{\mathrm{u,v}} \frac{\mathrm{u}^{\mathrm{T}} \sum_{m=1}^{t} \left(\mathrm{X}^{[m]}\right)^{\mathrm{T}} \mathrm{Y}_{\hat{k}^{[m]}} \mathrm{v}}{\sqrt{\mathrm{u}^{\mathrm{T}} \sum_{m=1}^{t} \left(\mathrm{X}^{[m]}\right)^{\mathrm{T}} \mathrm{Y}_{\hat{k}^{[m]}} \mathrm{u} \cdot \mathrm{v}^{\mathrm{T}} \mathrm{v}}} \\ &= \max_{\mathrm{u,v}} \frac{\mathrm{u}^{\mathrm{T}} C_{XY}^{[t]} \mathrm{v}}{\sqrt{\mathrm{u}^{\mathrm{T}} C_{XX}^{[t]} \mathrm{u} \cdot \mathrm{v}^{\mathrm{T}} \mathrm{v}}} \end{aligned} \tag{3}$$

$w_x^{[t+1]}$ and $w_y^{[t+1]}$ were the OMSCCA spatial filters. They were computed for the next trial. $C_{XX}^{[t]}$ or $C_{XY}^{[t]}$ was the sum of covariance matrices of multiple trials, and it can be updated whenever a new $\hat{k}^{[t]}$ was obtained by CCA.

$$\begin{aligned} C_{XX}^{[t]} &= C_{XX}^{[t-1]} + (X^{[t]})^{\mathrm{T}} X^{[t]} \\ C_{XY}^{[t]} &= C_{XY}^{[t-1]} + (X^{[t]})^{\mathrm{T}} Y_{\hat{k}^{[t]}} \end{aligned} \tag{4}$$

In our proposed eOACCA, the calculation of OMSCCA spatial filters also used data under other lighting conditions, so that the covariance matrix can contain enhanced information. As shown in formula (5):

$$\begin{aligned} C_{XX}^{t} &= C_{XX}^{bef} + (X^{[t]})^{\mathrm{T}} X^{[t]} = C_{XX}^{bef} + C_{XX}^{[t]} \\ C_{XY}^{t} &= C_{XY}^{bef} + (X^{[t]})^{\mathrm{T}} Y_{\hat{k}^{[t]}} = C_{XY}^{bef} + C_{XY}^{[t]} \end{aligned} \tag{5}$$

where C_{XX}^{bef}, C_{XY}^{bef} were the sum of covariance matrices generated by data under other lighting conditions. Formula (3) can be rewritten as:

$$\left\{w_x^{[t+1]}, w_y^{[t+1]}\right\} = \max_{\mathrm{u,v}} \frac{\mathrm{u}^{\mathrm{T}} \left(C_{XY}^{bef} + C_{XY}^{[t]}\right) \mathrm{v}}{\sqrt{\mathrm{u}^{\mathrm{T}} \left(C_{XX}^{bef} + C_{XX}^{[t]}\right) \mathrm{u} \cdot \mathrm{v}^{\mathrm{T}} \mathrm{v}}} \tag{6}$$

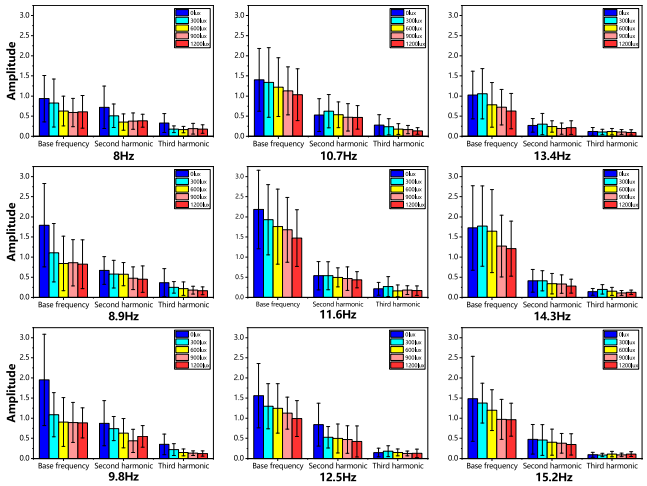

Fig. 4. Amplitude histograms at the nine stimulus frequencies. The unit was μV, and 3 harmonics were drawn in the figure.

Finally, we obtained three correlation coefficients:

$$\begin{aligned}\rho_{1k}^{[t]} &= CCA(\mathrm{X}^{[t]}, \mathrm{Y}_k)\\ \rho_{2k}^{[t]} &= CCA(\mathrm{X}^{[t]}\mathrm{u}_0^{[t]}, \mathrm{Y}_k)\\ \rho_{3k}^{[t]} &= corr(\mathrm{X}^{[t]}w_x^{[t]}, \mathrm{Y}_k w_y^{[t]})\end{aligned} \tag{7}$$

where *corr(a, b)* computed the correlation coefficient between two vectors a and b, CCA(A, B) calculated the correlation between two matrices A and B. Then we summed up these three coefficients as $\rho_k^{[t]} = \rho_{1k}^{[t]} + \rho_{2k}^{[t]} + \rho_{3k}^{[t]}$, and $\rho_k^{[t]}$ was the final coefficients of eOACCA.

III. Results

1) Amplitude and SNR of AR-SSVEP: Figure 4 showed the histogram of the AR-SSVEP response amplitudes under the 5 different light intensities. It can be observed that with the increase of the light intensity, the peak values of the target frequencies on the base frequency generally showed a downward trend, and this trend was more obvious at lower light intensities (≤600 lux). The overall downward trend was relatively small on the second harmonic, and no obvious change trend on the third harmonic. Besides, the AR-SSVEP responses were higher for the stimulus located in the center of the display interface than the other stimulus.

From Figure 5, it can be found that the average SNR gradually decreased with the increase of light intensity under the low light intensities (≤600 lux), and the downward trend was hardly observed under the high light intensities (>600 lux). Statistical analysis was then performed using paired t-test, and the results showed that the SNR under 0 lux light intensity was significantly higher than that under 600 lux ($p < 0.01$), 900 lux ($p < 0.01$) and 1200 lux ($p < 0.01$). The SNR under 300 lux was significantly higher than those under 600 lux ($p < 0.01$), 900 lux ($p < 0.01$) and 1200 lux ($p < 0.05$), and no significant difference was found between the other comparisons.

2) Target Recognition Accuracy and ITR: The AR-SSVEP recognition accuracies also showed a downward trend with the increase in light intensity, as shown in Figure 6. The highest accuracies of the two algorithms appeared in 0 lux

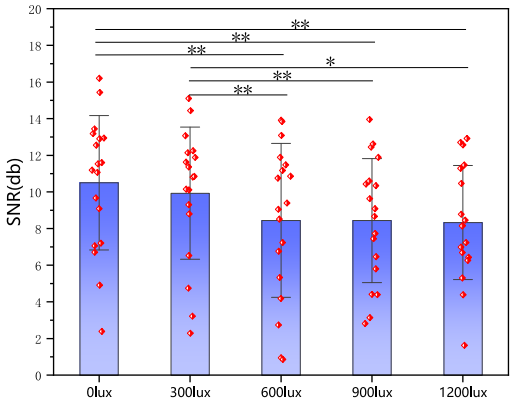

Fig. 5. SNRs under different light intensities. Each dot denoted the SNR of one of the 18 subjects (*: $p < 0.05$; **: $p < 0.01$).

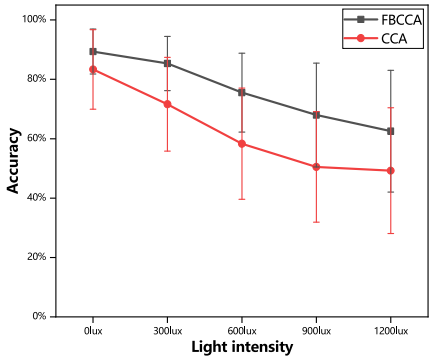

Fig. 6. Average accuracies of CCA and FBCCA under 5 light intensities.

light intensity, which was 89.35% of FBCCA and 83.33% of CCA respectively, and the lowest values appeared under 1200 lux light intensity, which was 62.53% of FBCCA and 49.24% of CCA respectively. In addition, with the increase of light intensity, the standard deviation of the accuracies became bigger, indicating that the subjects could not recognize the stimulus stably. Table I listed the accuracies of all subjects by using the FBCCA algorithm. The statistical test showed that there are significant accuracy differences ($p < 0.01$) between all the light intensities except for 0 lux and 300 lux ($p > 0.05$), and when the light intensity interval was bigger (≥600 lux), the difference is more significant ($p < 0.001$).

Since several subjects reported that the fixation process was affected by the spatial location of the flickering stimulus, we then calculated the recognition accuracies of the 9 targets. As shown in Figure 7, the accuracies of each target decreased with the increase in light intensity. When the light intensity was 0 lux, the accuracy of target 6 was up to 99.3%, and the accuracy of target 5 achieved the highest in the other light intensities, which were 98.58%, 97.18%, 91.61%, 84.62%, respectively. In particular, the accuracies of target 1 (8 Hz) and target 7(13.4 Hz) were lower than the other targets under all light intensities. With the increase of light intensities, the error rates increased sharply, and the minimum accuracies of the two targets were 5.59% at 1200 lux and 42.66% at 900 lux, respectively.

We further calculated the ITR under different light intensities, and the results were shown in Figure 8. The ITR

TABLE I
THE ACCURACIES ACHIEVED BY FBCCA OF 5 LIGHT INTENSITIES(%)

Sub	0lux	300lux	600lux	900lux	1200lux
S1	95.83	88.89	95.83	83.33	75.00
S2	91.67	63.89	40.28	20.83	11.11
S3	87.50	84.72	79.17	61.11	76.39
S4	95.83	94.44	84.72	86.11	79.17
S5	93.06	93.06	76.39	43.06	26.39
S6	84.72	81.94	75.00	70.83	75.00
S7	97.22	95.83	88.89	77.78	80.56
S8	98.61	91.67	86.11	83.33	80.56
S9	97.22	98.61	88.89	86.11	83.33
S10	80.56	76.39	66.67	70.83	50.00
S11	93.06	83.33	68.06	68.06	58.33
S12	88.89	69.44	64.20	72.22	68.06
S13	73.61	81.94	58.33	38.89	31.94
S14	90.28	83.33	71.43	69.44	58.33
S15	73.61	88.89	68.06	66.67	62.50
S16	83.33	79.17	83.33	72.22	70.83
S17	90.28	93.06	80.56	72.22	65.28
S18	93.06	87.50	83.33	80.56	72.84
AVE	**89.35**	**85.34**	**75.51**	**67.98**	**62.53**

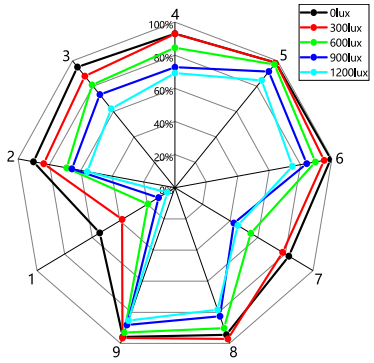

Fig. 7. Radar plot of single target recognition accuracy.

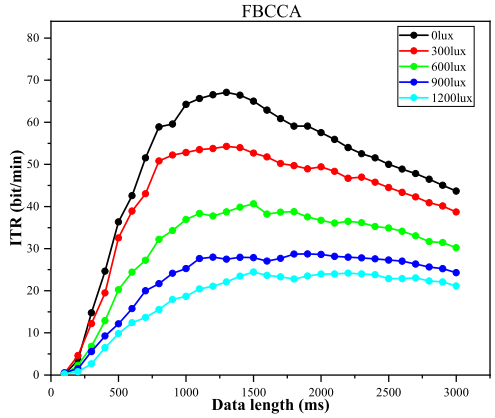

Fig. 8. ITRs of the 5 light density conditions. The abscissa was the length of EEG data used to recognize the target.

curve showed an upward trend at first, and then decreased after reaching the maximum value. The maximum value on 0 lux light intensity achieved 67.11 bits/min when the window length is 1300 ms. Among the 5 light intensities, both the ITR curve and the highest value showed a decreasing trend with the increase of light intensity.

A. Parameter Selection in eOACCA

In the eOACCA, two parameters affect the recognition accuracy of SSVEP, one is which target should be selected as the starting point of iterative learning? And the other is how to select data from other lighting conditions for auxiliary enhancement?

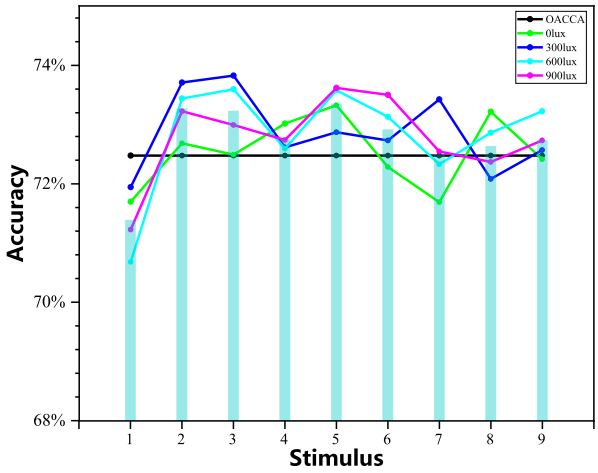

Fig. 9. The accuracies of 1200 lux with the first target optimization. The bars are the average of the four lighting conditions.

1) The Selection of the First Target: Since the OACCA method learned and iterated filters from the previous target recognition results, the accuracy of the previous target played a key role in the later data recognition. We recognized the EEG data at 1200 lux using all 9 targets separately at different light intensities, and the accuracy results were shown in Figure 9.

When using target 2, target 3 and target 5 as the starting point, the accuracies were higher than 72.48% of OACCA, and the accuracies were conversely lower than OACCA when using target 1. The average results among 0 lux, 300 lux, 600 lux and 900 lux further showed that the achieved accuracies were higher than OACCA when using all 9 targets as the starting point except target 1, and the target 5 which located in the center of the stimulus interface achieved the highest accuracy of 73.35%.

2) The Selection of Ancillary Lighting Condition Data: In OACCA, at the initial stage of calculation, both $S^{[0]}$ of PSF and $C_{XY}^{[0]}$, $C_{XY}^{[0]}$ of OMSCCA were set to 0 [22], which would make the filter learning time and the learning efficiency lower, and also affect the accuracy of target recognition at the early stage. Therefore, we provided initial values for $S^{[0]}$ and $C_{XX}^{[0]}$, $C_{XX}^{[0]}$ so that the learning and iteration of OACCA algorithm could achieve stable results faster. In this paper, we saved the S and C_{XX}^{bef}, C_{XY}^{bef} after iterative learning of data under other 4 lighting conditions in OACCA, and then used them as $S^{[0]}$ and $C_{XX}^{[0]}$, $C_{XY}^{[0]}$ of data under 1200 lux. According to 3.3.1, target 5 was used to optimize the first target.

As shown in Figure 10, the parameters obtained under all four auxiliary lighting conditions can improve the accuracy of 1200 lux data, and the obtained accuracies were 1.38%, 2.38%, 2.39% and 2.62% higher than that of OACCA. Among these four lighting conditions, the 900 lux, which was closest to the 1200 lux, achieved the highest accuracy.

Combined with the idea of iterative optimization, we further improved the iterative learning process of the eOACCA algorithm. We tried to iterate by using the data under 0 lux to provide the initial parameters for the 300 lux data, then

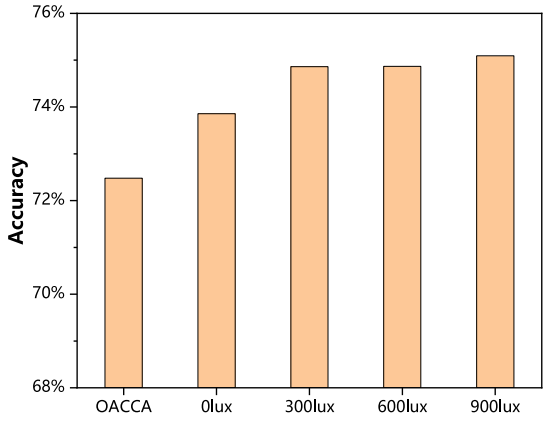

Fig. 10. The accuracies of 1200lux optimized with 0 lux, 300 lux, 600 lux and 900 lux data and the accuracy of OACCA algorithm.

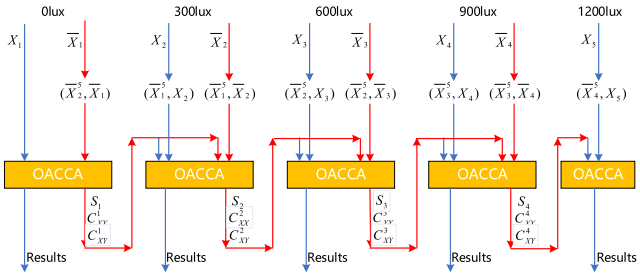

Fig. 11. The iterative learning process of the eOACCA algorithm.

using S and C_{XX}, C_{XY} generated from the 300 lux as the initial parameters for the 600 lux data, and continue to iterate until 1200 lux. As shown in Figure 11, when calculating the accuracy of data under 1200 lux, besides the information of data under 900 lux, the data information under 0 lux, 300 lux and 600 lux were also used in eOACCA.

B. The Recognition Performance of eOACCA

To verify the recognition performance of the eOACCA algorithm, we calculated the classification accuracy of data under the five lighting conditions by FBCCA, OACCA and eOACCA. Figure 12 showed that the accuracies of eOACCA were significantly higher than FBCCA and OACCA under strong light intensity (>600 lux), and the advantages were more obvious when the data length was short. Particularly, eOACCA significantly improved the accuracy under 1200 lux light intensity.

On the other hand, we analyzed the confusion matrices of FBCCA, OACCA and eOACCA under 600 lux, 900 lux and 1200 lux conditions. As shown in Figure 13, the accuracies of most of the targets had been improved after applying eOACCA, especially under high light intensity. Remarkably, the accuracies of target 1 were increased by 41.39%, 49.22% and 47.88% under the three high light intensities compared with FBCCA, and eOACCA had obvious improvements under 900 lux and 1200 lux compared with OACCA. The above results verified that the iterative learning process of eOACCA was effective when the light intensity changed drastically. Besides, the confusion matrix indicated that targets 1 and 7 are easily misclassified. Targets 1 and 7 were located at the upper

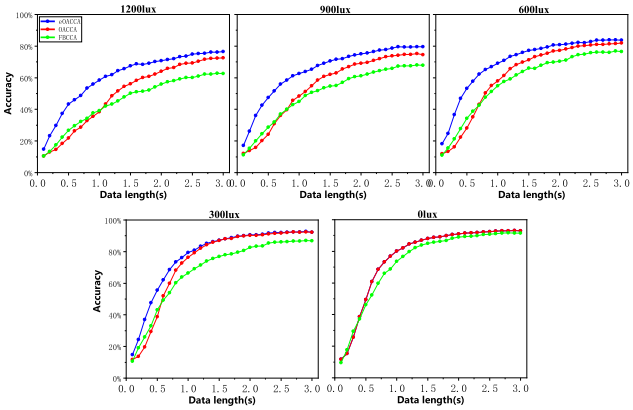

Fig. 12. Classification accuracies of FBCCA, OACCA and eOACCA under the five lighting conditions.

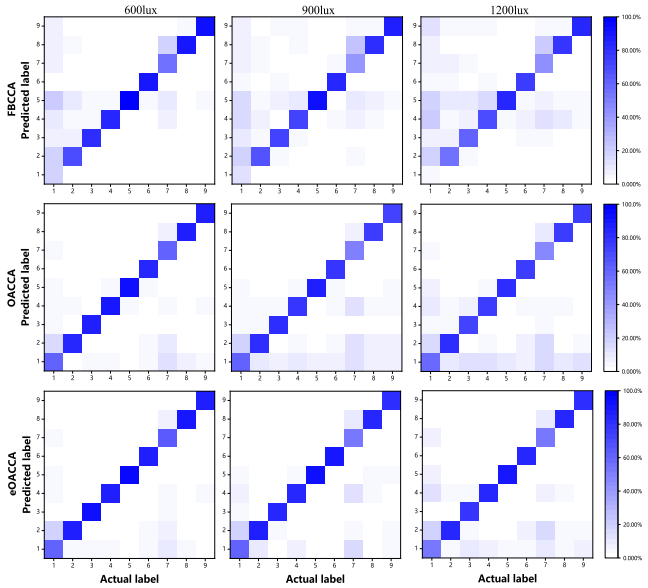

Fig. 13. Confusion matrix of the AR-SSVEP target recognition results under different light density conditions. The abscissa is the true label of the stimulus, the ordinate is the target recognition result.

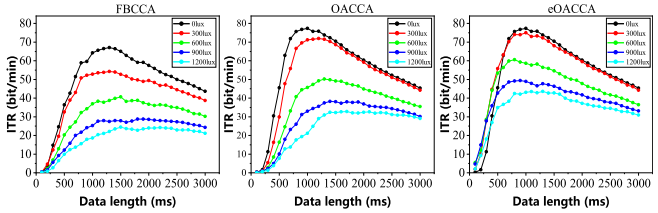

Fig. 14. ITR comparisons of the FBCCA, OACCA and eOACCA.

left and upper right of AR glass, and the light intensity seemed to have a greater impact on these two positions.

Finally, the ITRs of eOACCA were calculated, and compared with FBCCA and OACCA, as shown in Figure 14. The ITRs of eOACCA were higher than that of FBCCA and OACCA under all 5 light intensities when the light intensity was the same. The maximum ITRs achieved by eOACCA were 77.35 bits/min (1s, 0 lux), 74.99 bits/min (1s, 300 lux), 60.59 bits/min (0.8s, 600 lux), 49.39 bits/min (0.9s, 900 lux), and 43.47 bits/min (1.1s, 1200 lux), respectively.

IV. Discussion

Ambient brightness is a key factor affecting the development of AR-BCI in non-laboratory environments. In this study, the performance of AR-BCI was tested under various light intensities. It was discovered that when light intensity increased, the SSVEP response amplitude steadily weakened, which further reduced the recognition accuracy and ITR of AR-BCI. Since the light intensity is typically unstable, and the brightness is usually not as low as 0 or 300 lux in the BCI application environment outside the laboratory, it is necessary to investigate the causes of why the light intensity has a significant impact on the performance of AR-BCI and how to increase the recognition accuracy of AR-SSVEP under the high light intensity environments.

As far as we know, eye tracking technology is currently one of the important human-computer interaction methods in AR devices. It is reported that eye trackers also suffer from ambient brightness [35], on the one hand, rapid changes in light conditions directly reduce data quality [36], on the other hand, light conditions can indirectly introduce pupil-size artifacts by affecting the pupil shape [37]. Although the results of this work showed that the recognition performance of AR-SSVEP is also affected by light conditions, the research on AR-SSVEP has just started. If the recognition performance problem of AR-SSVEP in complex light environments is solved in the future, then SSVEP-BCI is expected to become an important means of human-computer interaction in AR devices.

A. The Effect of Stimulus Contrast

Contrast refers to the intensity of ambient contrast between the target flicker and the environment. Visual evoked potential (VEP) changes mainly originated from the response of the visual pathway to object edges in the visual cortex [38]. The sharpness of the object's edge was closely related to the contrast. High contrast could make the outline and details of the object clear, and the edge was more prominent. Many studies have shown that VEP exhibits a linear relationship with the logarithm of stimulus contrast [39], [40]. In the classical CS-SSVEP experiments, the stimulus paradigm was usually designed with a pure black or white background [41], [42], thus the contrast between the stimulus and the background was great and almost unaffected by ambient light. However, in the AR-SSVEP experiment, the stimulus was displayed by AR glass, the background of the stimulus was the real external environment, and the contrast between stimulus and background would be affected by the brightness of the external environment. During the experiment, as the light intensity grew, the total brightness of the background increased. Because the brightness of the stimulus remained constant, it greatly reduced the contrast between the stimulus and the background. Finally, the average response amplitude of the SSVEP was weakened.

The brightness of the flickering stimulus was another key factor, and it referred to the brightness provided by the optical system to the virtual image. A brighter flickering stimulus resulted in a significantly stronger SSVEP response [43]. Sufficient brightness can ensure the stimulus to own a good contrast, when there is a significant brightness difference between the stimulus and the background, the Mach effect will occur [44], which causes people to perceive the boundary of the stimulus brighter. However, the maximum brightness of the HoloLens1 AR glass used in this experiment was only 320 nits. According to the contrast calculation method described in [45], the obtained contrast of the stimulus were 3.76:1 and 3.07:1 at the light intensities of 900 lux and 1200 lux, while they did not reach the 5:1 ratio required for image readability specified in the paper [46].

The color of the stimulus also affected the contrast. On traditional CS-SSVEP, the contrast of the stimulus was hardly affected by ambient brightness, researchers were simply required to consider the signal quality and not the contrast when choosing colors. Related studies have shown that the red color could produce better SSVEP in the low-frequency band [47]. In the experiment, high-saturation (purity) red was used, this color was very bright and could create a striking contrast with its surroundings under lower light intensities. However, the individuals could view the outside environment while gazing at the stimulus since AR glass was used as the stimulus presentation device. Due to the possibility of ambient light directly passing through the virtual stimulus, the red saturation maybe decreased and the stimulus became blurry. It was known that cone cells were used primarily by the human visual system to collect external information in bright environments [48], and they were more sensitive to color. Thus, the visual signal produced by the stimulus on the retina could be weakened by a stimulus with insignificant colors, which lowered the quality of the SSVEP signal. In addition, the survey results of the subjects' subjective feelings also showed that the contrast between the red stimulus and the environment gradually decreased with the increase of the light intensity.

Lower contrast may affect the allocation of attentional resources when subjects perform the experimental task. The amplitude of SSVEP increased with the amount of attention resources devoted to the target stimulus [49], [50]. It had been confirmed that the accuracy under the condition of concentrating attention was higher than that of distracting attention [51]. As the light intensity increased, the contrast of the stimulus displayed by the AR glass was continuously reduced, making it difficult for individuals to devote more attention resources to the target stimulus. Therefore, the response of SSVEP was weakened and the recognition accuracy was reduced.

B. The Effect of Stimulus Layout on Performance

In Figure 13, it could be seen that the recognition accuracies of target 1 and 7 were significantly reduced, while the other targets were less affected, and this phenomenon might be related to the stimulus layout on the AR glass and the structure of the human eyes. On the one hand, it was reported that the brightness of the top left and top right areas were lower than the other areas when virtual objects displayed in Hololens1 AR glass. It made the brightness of targets 1 and 7 lower than the other targets, thus the subject's sight was easily attracted by the stimulus located at the center under strong

light intensity. As shown in Figure 13, target 1 and 7 were frequently misclassified as target 2, 4 and 5.

On the other hand, the visual cells in the human eyes were not uniformly distributed on the retina, and the macula located in the center of the retina contained more visual cells and had stronger ability to receive external visual stimuli. As a result, objects located in the center of the visual field could be seen more clearly by the human eyes [52]. In this experiment, as the brightness of the subject's visual field increased, the subject's pupil would gradually shrank to reduce the amount of light entering the eyes [53], and the macula would primarily be responsible for capturing visual information. However, the location of target 1 and target 7 were not in the center of the visual field, and the subjects were unable to change the projection position of the stimulus in the retina by moving their heads, which made the subjects have trouble focusing on the target stimulus clearly. Additionally, human eyes had a viewing angle of around 50° upwards and 70° downwards [54], making it more natural and comfortable for people to view the object below than the object above. This explained why there was little variation in the recognition accuracy of targets 3 and 9.

In addition, electrophysiological studies have shown that distinct EEG patterns emerge when the spatial position information of flickering stimuli in the visual field is mapped from retina to the visual cortex, it has been proved that such retinal mapping phenomenon can be used to design spatially-coded SSVEP-BCIs, and higher recognition accuracy has been achieved by classifying the distinct topographies of the spatially-coded SSVEP responses [55], [56]. We only used frequency information in the AR-SSVEP recognition in this work. It is speculated that the recognition accuracy of the targets at the corners can be improved if adding the spatial distribution information of elicited VEPs.

C. The Iterative Learning Process of eOACCA

According to the classification results shown in Section III-A, the eOACCA proposed in this work outperformed OACCA and FBCCA in terms of accuracy, especially for the data obtained in high-light conditions. The main idea of eOACCA was to use the data collected under favorable conditions to improve and optimize the data collected under unfavorable situations. Such scheme could be used not only for OACCA but also for other algorithms to improve the recognition performance of SSVEP collected in a variable environment. In the future online AR-BCI application, it is only necessary to add an additional light sensor to obtain the information of the external light intensity in real-time, then the iterative learning idea of the eOACCA algorithm can be applied to learn the filter parameters under low light intensity and optimize the filter parameters under strong light intensity in real-time.

In eOACCA, the first target optimization strategy similar as OACCA was used, but the starting point selection method for optimization was different. eOACCA fixedly selected target 5 under neighboring light intensities as the starting point for optimizing target light intensities, while OACCA started with random targets. For CS-SSVEP, there was not much difference in the recognition accuracy of different targets, therefore employing a random target as a starting point is not problematic. However, Figure 9 illustrated that the location of the target has a substantial impact on the recognition performance of AR-SSVEP, thus it is necessary to fix the starting point. In thecurrent study, target 5 was selected as the starting point because it achieved the highest recognition accuracy out of all 9 targets.

In addition, we performed data integration by superimposing filter parameters obtained from data under several lighting conditions, which was inspired by eTRCA [21], and then used them to calculate a new filter. Ideally, filters of different targets should be similar to each other, because the mixing coefficients from SSVEP source signals to scalp recordings could be considered similar within the used frequency range [57], [58]. Therefore, it was possible to integrate filters learned from other conditions to optimize the target condition. In eOACCA, the filter parameters under high light intensity were iteratively learned from the data under low light intensity, since the calculated target filter had been calibrated many times by data from favorable conditions, it could extract the characteristics of the target data more accurately. The classification results shown in Figure 12 proved that such filter ensemble mechanism was effective.

D. Potential Approaches to Improve the AR-BCI Performance in Strong Light Environments

An important obstacle for AR-BCI to go out of the laboratory is the inaccurate recognition of AR-SSVEP in the outdoor strong light environment. Since the brightness provided by AR glass is very weak compared with strong outdoor light, it may not be able to see the information displayed on the AR glass clearly under strong light, resulting in a failure to induce a strong SSVEP response. The human eye is more sensitive to images with high contrast. For the problem of reduced contrast between the flickering stimulus and the background caused by the increase in ambient brightness, we may be able to solve it by reducing the saturation of the virtual objects displayed on AR glass, for example, changing the color of the stimulus to black after the ambient brightness become strong. In addition, Xu et al.'s work inspired us that using the aVEPs evoked by lateral visual stimuli is a possible way to solve the problem of decreased recognition accuracy of AR-SSVEP in strong light environment [59].

According to the characteristics of AR-SSVEP, developing highly robust recognition algorithms is another important future research direction. The iterative learning optimization strategy proposed in this paper is just an attempt and provide ideas for subsequent improvements. The recognition algorithms of SSVEP mainly rely on CCA, which completes the recognition by calculating the correlation between the original data and the reference signal. Within this framework, using effective signal processing tools, such as empirical mode decomposition [60], empirical wavelet transform [61], variational mode decomposition [62], independent component analysis, et al., to preprocess the raw signals firstly, removing artifacts as much as possible, then applying CCA for recognition based on the SSVEP components that were extracted after

preprocessing, may help to improve the recognition accuracy of AR-SSVEP. Using the learned spatial filters to precisely extract SSVEP components from EEG is another option to increase the accuracy of SSVEP recognition, such as [34], [63]. Thus, designing more effective spatial filters is another potential way to improve the AR-SSVEP recognition accuracy under strong light.

In addition, the negative impact of strong light on AR-SSVEP can be improved by adding some physical protection. For instance, a photochromic glasses lens can be installed on the outside of the lens of AR glass, which can automatically reduce the light transmittance under strong external light, and increase the light transmittance when the light intensity drops. In this way, the light entering the human eyes can be reduced in a strong light environment, and the response strength of AR-SSVEP can be improved, and at the same time, the human eye's perception of the external environment will not be affected in a low light environment.

V. Conclusion

The development of BCI technology has reached the critical stage of going out of the laboratory. AR technology can provide a huge impetus for the application of BCI, but it still faces some problems when combing with BCI. Current work analyzed the recognition performance variations of the AR-SSVEP under different light intensities. The findings demonstrated that when light intensity increases, the response intensity of AR-SSVEP gradually decreases, and the recognition accuracy exhibits a similar declining trend, too. In the experiment, the selection of lighting conditions could cover the illumination conditions of most scenes, thus the results have guiding significance for the application of AR-BCI in actual scenes. We further proposed an iterative learning optimization strategy to improve the performance of AR-SSVEP under strong light. Experimental results showed that the proposed eOACCA outperforms FBCCA and OACCA, indicating that our proposed optimization strategy was feasible.

To the best of our knowledge, this is the first study discussing the light intensity effect on AR-BCI. Our work provides theoretical guidance and technical support for AR-BCI to go out of the laboratory by studying the phenomenon and causes of AR-BCI performance variations under various light intensities, and proposing an improved recognition algorithm. The optimization strategy proposed in this paper is also valuable for the improvement of SSVEP recognition algorithms under other unstable situations.

References

[1] J. Wolpaw, N. Birbaumer, D. McFarland, G. Pfurtscheller, and T. Vaughan, "Brain–computer interfaces for communication and control," *Clin. Neurophys.*, vol. 113, no. 6, pp. 767–791, 2002.

[2] D. Yao et al., "Correction to: Bacomics: A comprehensive cross area originating in the studies of various brain–apparatus conversations," *Cognit. Neurodyn.*, vol. 14, pp. 425–442, Aug. 2022.

[3] R. B. Silberstein, "Steady state visually evoked potential, brain resonances and cognitive processes," *Int. J. Psychophysiol.*, vol. 35, no. 1, p. 5, Feb. 2000.

[4] G. Zhang et al., "Computational exploration of dynamic mechanisms of steady state visual evoked potentials at the whole brain level," *NeuroImage*, vol. 237, Aug. 2021, Art. no. 118166.

[5] S. Gao, Y. Wang, X. Gao, and B. Hong, "Visual and auditory brain–computer interfaces," *IEEE Trans. Biomed. Eng.*, vol. 61, no. 5, pp. 1436–1447, May 2014.

[6] Y. Zhang et al., "Hierarchical feature fusion framework for frequency recognition in SSVEP-based BCIs," *Neural Netw.*, vol. 119, pp. 1–9, Nov. 2019.

[7] Y. Zhang, P. Xu, T. Liu, J. Hu, R. Zhang, and D. Yao, "Multiple frequencies sequential coding for SSVEP-based brain-computer interface," *PLoS ONE*, vol. 7, no. 3, Mar. 2012, Art. no. e29519.

[8] Y. Wang, K. Li, X. Zhang, J. Wang, and R. Wei, "Research on the application of augmented reality in SSVEP-BCI," in *Proc. 6th Int. Conf. Comput. Artif. Intell.*, Apr. 2020, pp. 505–509.

[9] R. Furlan, "The future of augmented reality: Hololens–Microsoft's AR headset shines despite rough edges," *IEEE Spectr.*, vol. 53, no. 6, p. 21, Jun. 2016.

[10] R. Azuma, Y. Baillot, R. Behringer, S. Feiner, S. Julier, and B. MacIntyre, "Recent advances in augmented reality," *IEEE Comput. Graph. Appl.*, vol. 21, no. 6, pp. 34–47, Nov. 2001.

[11] T. P. Caudell and D. W. Mizell, "Augmented reality: An application of heads-up display technology to manual manufacturing processes," in *Proc. 25th Hawaii Int. Conf. Syst. Sci.*, 1992, pp. 1–4.

[12] M. Xu, F. He, T.-P. Jung, X. Gu, and D. Ming, "Current challenges for the practical application of electroencephalography-based brain–computer interfaces," *Engineering*, vol. 7, no. 12, pp. 1710–1712, Dec. 2021.

[13] H. Si-Mohammed et al., "Towards BCI-based interfaces for augmented reality: Feasibility, design and evaluation," *IEEE Trans. Vis. Comput. Graph.*, vol. 26, no. 3, pp. 1608–1621, Mar. 2020.

[14] Y. Ke, P. Liu, X. An, X. Song, and D. Ming, "An online SSVEP-BCI system in an optical see-through augmented reality environment," *J. Neural Eng.*, vol. 17, no. 1, Feb. 2020, Art. no. 016066.

[15] X. Zhao, C. Liu, Z. Xu, L. Zhang, and R. Zhang, "SSVEP stimulus layout effect on accuracy of brain-computer interfaces in augmented reality glasses," *IEEE Access*, vol. 8, pp. 5990–5998, 2020.

[16] R. Zhang et al., "The effect of stimulus number on the recognition accuracy and information transfer rate of SSVEP–BCI in augmented reality," *J. Neural Eng.*, vol. 19, no. 3, Jun. 2022, Art. no. 036010.

[17] A. Ravi, J. Lu, S. Pearce, and N. Jiang, "Enhanced system robustness of asynchronous BCI in augmented reality using steady-state motion visual evoked potential," *IEEE Trans. Neural Syst. Rehabil. Eng.*, vol. 30, pp. 85–95, 2022.

[18] D. Zhang et al., "Machine-vision fused brain machine interface based on dynamic augmented reality visual stimulation," *J. Neural Eng.*, vol. 18, no. 5, Oct. 2021, Art. no. 056061.

[19] Z. Lin, C. Zhang, W. Wu, and X. Gao, "Frequency recognition based on canonical correlation analysis for SSVEP-based BCIs," *IEEE Trans. Biomed. Eng.*, vol. 53, no. 12, pp. 2610–2614, Dec. 2006.

[20] X. Chen, Y. Wang, S. Gao, T.-P. Jung, and X. Gao, "Filter bank canonical correlation analysis for implementing a high-speed SSVEP-based brain–computer interface," *J. Neural Eng.*, vol. 12, no. 4, Aug. 2015, Art. no. 046008.

[21] M. Nakanishi, Y. Wang, X. Chen, Y. Wang, X. Gao, and T.-P. Jung, "Enhancing detection of SSVEPs for a high-speed brain speller using task-related component analysis," *IEEE Trans. Biomed. Eng.*, vol. 65, no. 1, pp. 104–112, Jan. 2018.

[22] C. M. Wong et al., "Online adaptation boosts SSVEP-based BCI performance," *IEEE Trans. Biomed. Eng.*, vol. 69, no. 6, pp. 2018–2028, Jun. 2022.

[23] Y. Chen, C. Yang, X. Chen, Y. Wang, and X. Gao, "A novel training-free recognition method for SSVEP-based BCIs using dynamic window strategy," *J. Neural Eng.*, vol. 18, no. 3, Mar. 2021, Art. no. 036007.

[24] I. Volosyak, "SSVEP-based Bremen–BCI interface—Boosting information transfer rates," *J. Neural Eng.*, vol. 8, no. 3, Jun. 2011, Art. no. 036020.

[25] P. Yuan, X. Chen, Y. Wang, X. Gao, and S. Gao, "Enhancing performances of SSVEP-based brain–computer interfaces via exploiting inter-subject information," *J. Neural Eng.*, vol. 12, no. 4, Aug. 2015, Art. no. 046006.

[26] B. Lee et al., "Key issues and technologies for AR/VR head-mounted displays," *Proc. SPIE, Adv. Display Technol. X*, vol. 11304, p. 1130402, 2020.

[27] E. H. Land, "Retinex theory of color-vision," *Sci. Amer.*, vol. 237, no. 6, p. 108, 1977.

[28] B. C. Kress and W. J. Cummings, "Invited paper: Towards the ultimate mixed reality experience: Hololens display architecture choices," in *Proc. SID Symp. Dig. Tech. Papers*, May 2017, vol. 48, no. 1, pp. 127–131.

[29] N. V. Manyakov, N. Chumerin, A. Robben, A. Combaz, M. van Vliet, and M. M. Van Hulle, "Sampled sinusoidal stimulation profile and multichannel fuzzy logic classification for monitor-based phase-coded SSVEP brain–computer interfacing," *J. Neural Eng.*, vol. 10, no. 3, Jun. 2013, Art. no. 036011.

[30] X. Chen, Z. Chen, S. Gao, and X. Gao, "A high-ITR SSVEP-based BCI speller," *Brain-Comput. Interfaces*, vol. 1, nos. 3–4, pp. 181–191, Mar. 2014.

[31] S. Mehrotra, S. Basukala, and S. Devarakonda, "Effective lighting design standards impacting patient care: A systems approach," *J. Biosci. Med.*, vol. 3, no. 11, pp. 54–61, 2015.

[32] J. R. Wolpaw, H. Ramoser, D. J. McFarland, and G. Pfurtscheller, "EEG-based communication: Improved accuracy by response verification," *IEEE Trans. Rehabil. Eng.*, vol. 6, no. 3, pp. 326–333, Sep. 1998.

[33] K. F. Lao, C. M. Wong, Z. Wang, and F. Wan, "Learning prototype spatial filters for subject-independent SSVEP-based brain–computer interface," in *Proc. IEEE Int. Conf. Syst., Man, Cybern. (SMC)*, Oct. 2018, pp. 485–490.

[34] C. M. Wong et al., "Learning across multi-stimulus enhances target recognition methods in SSVEP-based BCIs," *J. Neural Eng.*, vol. 17, no. 1, Jan. 2020, Art. no. 016026.

[35] K. Holmqvist et al., "Eye tracking: Empirical foundations for a minimal reporting guideline," *Behav. Res. Methods*, vol. 55, no. 1, pp. 364–416, Apr. 2022.

[36] W. Fuhl, M. Tonsen, A. Bulling, and E. Kasneci, "Pupil detection for head-mounted eye tracking in the wild: An evaluation of the state of the art," *Mach. Vis. Appl.*, vol. 27, no. 8, pp. 1275–1288, Nov. 2016.

[37] I. T. C. Hooge, D. C. Niehorster, R. S. Hessels, D. Cleveland, and M. Nyström, "The pupil-size artefact (PSA) across time, viewing direction, and different eye trackers," *Behav. Res. Methods*, vol. 53, no. 5, pp. 1986–2006, Oct. 2021.

[38] D. H. Hubel and T. N. Wiesel, "Receptive fields, binocular interaction and functional architecture in the cat's visual cortex," *J. Physiol.*, vol. 160, pp. 106–154, 1962.

[39] F. W. Campbell and L. Maffei, "Electrophysiological evidence for the existence of orientation and size detectors in the human visual system," *J. Physiol.*, vol. 207, no. 3, pp. 635–652, May 1970.

[40] F. W. Campbell and J. J. Kulikowski, "The visual evoked potential as a function of contrast of a grating pattern," *J. Physiol.*, vol. 222, no. 2, pp. 345–356, 1972.

[41] E. Yin, Z. Zhou, J. Jiang, F. Chen, Y. Liu, and D. Hu, "A speedy hybrid BCI spelling approach combining P300 and SSVEP," *IEEE Trans. Biomed. Eng.*, vol. 61, no. 2, pp. 473–483, Feb. 2014.

[42] M. Xu, J. Han, Y. Wang, T.-P. Jung, and D. Ming, "Implementing over 100 command codes for a high-speed hybrid brain–computer interface using concurrent P300 and SSVEP features," *IEEE Trans. Biomed. Eng.*, vol. 67, no. 11, pp. 3073–3082, Nov. 2020.

[43] A. Duszyk et al., "Towards an optimization of stimulus parameters for brain–computer interfaces based on steady state visual evoked potentials," *PLoS ONE*, vol. 9, no. 11, Nov. 2014, Art. no. e112099.

[44] L. Pessoa, "Mach bands: How many models are possible? Recent experimental findings and modeling attempts," *Vis. Res.*, vol. 36, no. 19, pp. 3205–3227, Oct. 1996.

[45] Y.-H. Lee, T. Zhan, and S.-T. Wu, "Prospects and challenges in augmented reality displays," *Virtual Reality Intell. Hardware*, vol. 1, no. 1, pp. 10–20, Feb. 2019.

[46] H. Chen, G. Tan, and S.-T. Wu, "Ambient contrast ratio of LCDs and OLED displays," *Opt. Exp.*, vol. 25, no. 26, p. 33643, 2017.

[47] D. Regan, "An effect of stimulus colour on average steady-state potentials evoked in man," *Nature*, vol. 210, no. 5040, pp. 1056–1057, Jun. 1966.

[48] R. Ward et al., "Non-photopic and photopic visual cycles differentially regulate immediate, early, and late phases of cone photoreceptor-mediated vision," *J. Biol. Chem.*, vol. 295, no. 19, pp. 6482–6497, May 2020.

[49] Y. Joon Kim, M. Grabowecky, K. A. Paller, K. Muthu, and S. Suzuki, "Attention induces synchronization-based response gain in steady-state visual evoked potentials," *Nature Neurosci.*, vol. 10, no. 1, pp. 117–125, Jan. 2007.

[50] S. T. Morgan, J. C. Hansen, and S. A. Hillyard, "Selective attention to stimulus location modulates the steady-state visual evoked potential," *Proc. Nat. Acad. Sci. USA*, vol. 93, no. 10, pp. 4770–4774, 1996.

[51] P. Toffanin, R. de Jong, A. Johnson, and S. Martens, "Using frequency tagging to quantify attentional deployment in a visual divided attention task," *Int. J. Psychophysiol.*, vol. 72, no. 3, pp. 289–298, Jun. 2009.

[52] D. A. Tipton, "A review of vision physiology," *Aviation, Space, Environ. Med.*, vol. 55, no. 2, pp. 145–149, 1984.

[53] Y. Suzuki, T. Minami, and S. Nakauchi, "Pupil constriction in the glare illusion modulates the steady-state visual evoked potentials," *Neuroscience*, vol. 416, pp. 221–228, Sep. 2019.

[54] W. Brian et al., "Field of view: Not just a number," *Digit. Opt. Immersive Displays*, vol. 10676, Jan. 2018, Art. no. 1067604.

[55] A. Maye, D. Zhang, and A. K. Engel, "Utilizing retinotopic mapping for a multi-target SSVEP BCI with a single flicker frequency," *IEEE Trans. Neural Syst. Rehabil. Eng.*, vol. 25, no. 7, pp. 1026–1036, Jul. 2017.

[56] J. Chen, A. Maye, A. K. Engel, Y. Wang, X. Gao, and D. Zhang, "Simultaneous decoding of eccentricity and direction information for a single-flicker SSVEP BCI," *Electronics*, vol. 8, no. 12, p. 1554, Dec. 2019.

[57] J. M. Ales and A. M. Norcia, "Assessing direction-specific adaptation using the steady-state visual evoked potential: Results from EEG source imaging," *J. Vis.*, vol. 9, no. 7, pp. 1–8, Jul. 2009.

[58] R. Srinivasan, F. A. Bibi, and P. L. Nunez, "Steady-state visual evoked potentials: Distributed local sources and wave-like dynamics are sensitive to flicker frequency," *Brain Topogr.*, vol. 18, no. 3, pp. 167–187, Spring 2006.

[59] M. Xu, X. Xiao, Y. Wang, H. Qi, T.-P. Jung, and D. Ming, "A brain–computer interface based on miniature-event-related potentials induced by very small lateral visual stimuli," *IEEE Trans. Biomed. Eng.*, vol. 65, no. 5, pp. 1166–1175, May 2018.

[60] N. E. Huang et al., "The empirical mode decomposition and the Hilbert spectrum for nonlinear and non-stationary time series analysis," *Proc. Roy. Soc. London, A, Math., Phys. Eng. Sci.*, vol. 454, no. 1971, pp. 903–995, 1998.

[61] J. Gilles, "Empirical wavelet transform," *IEEE Trans. Signal Process.*, vol. 61, no. 16, pp. 3999–4010, May 2013.

[62] L. Chang, R. Wang, and Y. Zhang, "Decoding SSVEP patterns from EEG via multivariate variational mode decomposition-informed canonical correlation analysis," *Biomed. Signal Process. Control*, vol. 71, Jan. 2022, Art. no. 103209.

[63] B. Liu, X. Chen, N. Shi, Y. Wang, S. Gao, and X. Gao, "Improving the performance of individually calibrated SSVEP-BCI by task-discriminant component analysis," *IEEE Trans. Neural Syst. Rehabil. Eng.*, vol. 29, pp. 1998–2007, 2021.